Structural and optical analysis of amorphous TiO_2 films obtained by sol-gel process and deposited by spin coating on PET/ITO at room temperature

C. Montero-Tavera[a], M. Loeza-Poot[a], M. Oviedo-Mendoza[b], J. Moreno-Palmerín[c], W. B. Rojas-Salinas[a], F. Caballero-Briones[d], M. Zapata-Torres[e], and E. N. Hernández-Rodríguez[a,*]

[a]*Universidad de Guanajuato, carretera Salamanca-Valle de Santiago Km. 3.5+1.8, Comunidad de Palo Blanco, Salamanca, Guanajuato, México.*
[b]*Universidad Politécnica de Guanajuato, Av. Universidad Sur 1001, P.C. 38496, Cortazar, Guanajuato, México.*
[c]*Departamento de Minas, Metalurgia y Geología, Universidad de Guanajuato, Ex Hacienda de San Matías S/N, P.C. 36020, Guanajuato, Guanajuato, México.*
[d]*Instituto Politécnico Nacional, GESMAT, CICATA Altamira, 89600, Tamaulipas, México.*
[e]*Instituto Politécnico Nacional, CICATA-Legaria, Ciudad de México, México.*
[*]*e-mail: noe.hernandez@ugto.mx.*

Received 16 May 2025; accepted 11 November 2025

In this work, we proposed a methodology based on the spin coating technique for the deposition of amorphous TiO_2 layers obtained by the sol-gel method onto flexible PET/ITO substrates intended for application in flexible organic solar cells (FOSCs). Spin-coated TiO_2 layers were used to investigate the influence of their optical and structural properties on the light absorption behavior of the P3HT:PCBM active layer, to integrate the photovoltaic system PET/ITO/TiO_2/P3HT:PCBM. Raman spectroscopy confirmed the amorphous nature of TiO_2. The average particle size was 86 nm, according to SEM results. UV-Vis measurements of TiO_2 layers showed a transmittance greater than 65% and a bandgap of 3.77 eV, which corresponds to the bandgap of amorphous TiO_2, making them a novel material for electromagnetic radiation to reach the P3HT:PCBM absorber layer and generate excitons within it. Regions of high light absorbance (300-550 nm) and weak light absorbance (650-900 nm) were identified. FT-IR spectra revealed the characteristic absorbance bands of Ti-O at 523 cm^{-1} and Ti-O-Ti at 434 cm^{-1}. AFM images revealed a uniform distribution of TiO_2 onto PET/ITO and the typical P3HT:PCBM microstructure This methodology enables the deposition of TiO_2 layers at room temperature without the use of any additional chemical bonding agents, which is a key factor for low-temperature fabrication of FOSCs.

Keywords: Flexible substrate; amorphous TiO_2; spin-coating; room temperature.

DOI: https://doi.org/10.31349/RevMexFis.72.041001

1. Introduction

Titanium dioxide TiO_2 is one of the most widely used materials due to its physicochemical properties [1]. The synthesis and research of TiO_2 thin films have been studied for more than half a century. TiO_2 presents three crystallographic phases: anatase, rutile, and brookite [2]. Among them, the anatase phase is of great interest because of its structural stability below 800°C [3,4]. The high percentage of transmittance of visible electromagnetic radiation and electron transport makes it suitable for use as part of photovoltaic systems for the generation of clean energy. However, other researchers have focused on understanding the structural and optical properties of amorphous TiO_2 because it is a way to obtain a less processed and cheaper material [5].

The generation of clean energy [6-9] has been the focus of extensive research in recent decades because it does not have a negative impact on the environment. Since the mechanism of converting solar energy into electric current was understood, a wide variety of solar cells began to be developed [10-12]. Polymer-based organic solar cells (OSCs) have attracted great interest due to several advantages such as low cost, flexibility, lightweight, and easy fabrication [13-15] compared to inorganic solar cells. However, OSCs exhibit low energy conversion efficiency and reduced stability [16].

In general, a flexible organic solar cell (FOSC) uses a substrate transparent to visible electromagnetic radiation, a transparent conductive layer, a light-absorbing layer based on semiconducting polymers where the conversion of solar energy into electric current takes place, a hole transport layer, and a metallic conductive layer. The most commonly used polymers to form the absorber layer are P3HT (Poly(3-hexylthiophene-2,5-diyl)) and PCBM (6,6-phenyl-C_{61}-butyric acid methyl ester), acting as donor and acceptor components, respectively, to form the P3HT:PCBM absorber layer. This polymer-fullerene system, in the form of a bulk heterojunction, is widely used in organic solar cells due to its compatibility and well-known physicochemical behavior [17,18]. Other photovoltaic cell configurations have been reported in which the P3HT:PCBM system incorporates semi-

conducting nanoparticles of various kinds to improve light absorption properties [19-21].

In order to achieve competitive photoconversion efficiency, the buffer layers between the electrodes and the absorber layer play an important role in OSCs. TiO_2 and ZnO have been the subject of many experimental studies as interlayers between ITO and P3HT:PCBM in OSCs with inverted configuration [22,23], and TiO_2 has shown good results due to properties such as high electron mobility, chemical stability under environmental conditions, and high transparency [24]. However, in flexible OSCs, buffer layer fabrication becomes a challenge because in FOSCs the polymeric substrate (PET) imposes restrictions on the processing temperature during TiO_2 layer fabrication [25]. Therefore, conventional and well-established techniques for thin-film fabrication cannot be employed. New methodologies for producing TiO_2 layers at low temperatures (near room temperature) must be developed, ensuring that the optical and electrical properties of the obtained TiO_2 layers are suitable for FOSC performance.

Therefore, in this research, we proposed a methodology to deposit amorphous TiO_2 thin films at room temperature onto a flexible, organic, and transparent PET/ITO (Polyethylene Terephthalate/Indium Tin Oxide) substrate. The spin-coating technique was developed to increase light absorption in the P3HT:PCBM active layer. It is highlighted that no chemical bonding agents were used to deposit TiO_2 films onto PET/ITO because such agents could act as scattering centers for electromagnetic radiation, which is undesirable for photovoltaic devices. Other methods to deposit crystalline TiO_2 have been reported [26,27], but these involve high temperatures and complex synthesis conditions that are not suitable for the PET/ITO substrate employed in this investigation, mainly because PET cannot withstand high processing temperatures.

2. Materials and methods

2.1. Materials

The materials used in this investigation were anhydrous titanium (IV) chloride ($TiCl_4$, Sigma-Aldrich 99.9%), P3HT (poly(3-hexylthiophene-2,5-diyl), Sigma-Aldrich, 99.995%), PCBM (6,6-phenyl-C_{61}-butyric acid methyl ester, Sigma-Aldrich, 99%), chlorobenzene (CB) (Sigma-Aldrich 98.9%), 96% (v/v) ethanol (EQUIBA), ammonium hydroxide (NH_4OH, Karal, 30%), H_2O_2 (Golden Bell, 50%), distilled water, and commercial PET/ITO (60 Ω/sq) with thicknesses of 0.127 mm and 130 nm, respectively (Sigma-Aldrich).

2.2. Synthesis of materials

To synthesize TiO_2 using the sol-gel technique, 2 mL of $TiCl_4$ was mixed with 200 mL of distilled water at 0°C and stirred for 30 min. After this period, the sample was allowed to reach room temperature. Then, NH_4OH was added until the pH reached a value between 8 and 9, forming $Ti(OH)_4$ (white gel). The resulting $Ti(OH)_4$ was washed for several hours. Eight grams were then dispersed in 800 mL of distilled water containing 11.2 mL of H_2O_2, and a cloudy yellow solution was observed. This mixture was stirred at room temperature until it turned transparent. Subsequently, it was heated at 98-100°C until the desired volume of TiO_2 was formed [28]. This mixture (TiO_2 synthesized by sol-gel) was deposited by spin coating onto flexible transparent PET/ITO substrates with a 1 in^2 area previously washed in an ultrasonic bath using soap, methyl alcohol, and distilled water (8 minutes in each stage). A volume of 600 μL of TiO_2 (obtained by sol-gel) was deposited onto the flexible substrates, and then a rotation speed of 100 rpm was applied for 10 s; afterward, the speed was increased to 600 rpm for 20 s. Finally, the obtained layers were annealed at 120°C for 20 minutes to evaporate residual water.

The P3HT:PCBM absorbent layer was synthesized by mixing P3HT:PCBM and CB in a ratio of 3:1, stirring and heating at 53°C for 18 hours in a water bath. Finally, the mixture was spin-coated onto PET/ITO/TiO_2 structures at room temperature as reported in Ref. [29].

2.3. Materials characterization

Raman spectroscopy analysis was performed using a GemRam BW Tek (300 mW, 785 nm), scanning from 100 to 900 cm^{-1}. Scanning Electron Microscopy (SEM) measurements were carried out with a JEOL JSM-6010 PLUS/LA. Optical characterization was conducted using an Ocean Optics UV-Vis spectrophotometer (US 4000-XR1-ES), scanning from 300 to 900 nm to obtain the transmission spectra. The FT-IR analysis was performed with a GX spectrometer (Perkin Elmer), using specular reflectance with a 30° angle, a 3/8 in diameter aperture mask, and 4 cm^{-1} resolution. TT-AFM Workshop in intermittent tapping mode was used to obtain Atomic Force Microscopy (AFM) images of a P3HT:PCBM blend deposited on the TiO_2 layer.

3. Results and discussion

The hydrolysis of $TiCl_4$ produces TiO_2, resulting in an acidic mixture due to the presence of HCl:

$$TiCl_4 + H_2O \iff TiO_2 + 4HCl, \quad (1)$$

Ti^{4+} ions are converted to $Ti(OH)_4$ gel with the addition of NH_4OH until the pH increases to 8-9 (basic mixture). The gel is dispersed in distilled water and hydrogen peroxide is added, producing two reactions:

$$Ti(OH)_4 \iff TiO_2^+ + 2OH^- + 2H_2O, \quad (2)$$

$$TiO_2^+ + H_2O_2 \iff [TiO(H_2O_2)]^{2+}. \quad (3)$$

As indicated in reaction (2), the addition of distilled water to $Ti(OH)_4$ gel causes a hydrolysis reaction that shifts to the right-hand side, and $Ti(OH)_4$ gradually dissolves into TiO_2,

hydroxyl radicals, and water [30]. In reaction (3), it is observed that hydrogen peroxide exhibits strong coordination with TiO_2^+. The decomposition of H_2O_2 allowed the equilibrium of reaction (3) to shift to the right side, forming the pertitanate ion $[TiO(H_2O_2)]^{2+}$; because the decomposition rate of the ion was very slow, the TiO_2 particles formed by the decomposition of $[TiO(H_2O_2)]^{2+}$ were very small and uniform. As a result, a stable TiO_2 solution was formed. Therefore, it can be used as a coating solution on a PET/ITO substrate. TiO_2 obtained by sol-gel was used to fabricate thin layers by the spin-coating technique. PET/ITO commercial substrates were used, because they can be integrated into OSC devices.

3.1. Structural characterization

Figure 1a) presents a top-view SEM image of a representative amorphous TiO_2 layer, showing a uniform surface, free of cracks and holes, and therefore suitable for use in solar cell devices. The TiO_2 structure is granular, as reported in previous investigations [31], with an average particle size of 0.086 μm (86 nm). [See Fig. 1a)]. This value was calculated from image analysis using the Fiji software from ImageJ. Figure 1b) displays a histogram of the particle size distribution determined from SEM micrographs. The data indicate a variation in particle size, with a greater presence of 8 nm and 90 nm grains. We associate this granular structure with the basic pH ($\approx$ 8) of the $Ti(OH)_4$ gel, which promotes the formation of large particle sizes, as reported in Ref. [28]. Moreover, the annealing temperature of 120 °C is insufficient to form crystalline grains, as documented in Ref. [32].

The AFM images for the TiO_2 film deposited at room temperature are presented in Figs 2a) and 2b). Figure 2a) reveals smooth and homogeneous TiO_2 surfaces. A uniform distribution of TiO_2 across the surface is observed, consistent with the SEM image, without any visible cracks or discontinuities that could affect the subsequent deposition of the P3HT:PCBM active layer for solar cell fabrication. Figure 2b) illustrates the composition of TiO_2 spin-coated on the substrate. It can be seen that the same TiO_2 composition is present throughout the sample, demonstrating that the spin coating technique is adequate to obtain the PET/ITO/TiO_2 structures.

XRD spectra from TiO_2 films did not show any diffraction peaks, suggesting that TiO_2 is amorphous [33]. It was confirmed by Raman spectroscopy of TiO_2 spin-coated onto PET/ITO presented in Fig. 3, where no vibrational modes corresponding to crystalline TiO_2 were detected (measurements were conducted at many different zones of the sample surface) [34], but PET/ITO substrate vibrational modes can be seen at 128 cm^{-1}, 633 cm^{-1}, 703 cm^{-1}, and 860 cm^{-1} in agreement with the literature [35]. Additionally, FT-IR

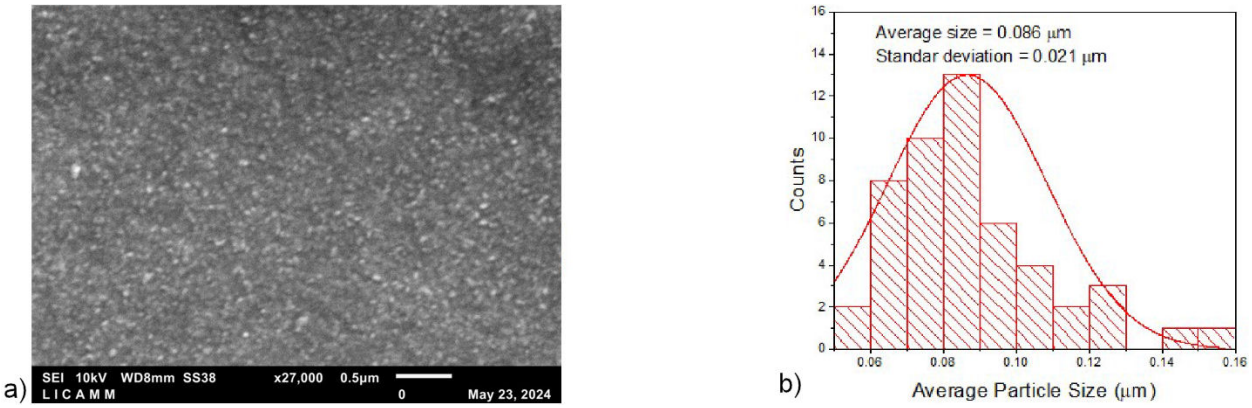

FIGURE 1. a) SEM surface image of amorphous TiO_2 deposited on a PET/ITO substrate, b) histogram of the particle size distribution.

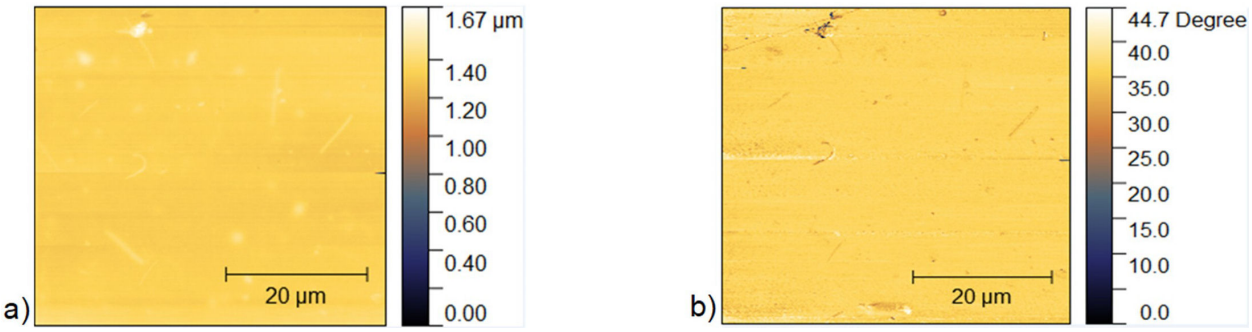

FIGURE 2. AFM images of TiO_2. a) Topography image revealing a smooth layer, b) Phase image indicating the same composition in the layer.

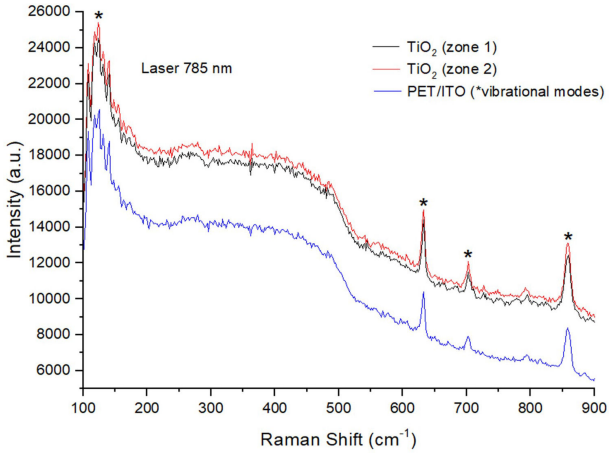

FIGURE 3. Raman spectrum shows only the vibrational modes of PETITO substrates. No characteristic TiO_2 vibrational modes are observed.

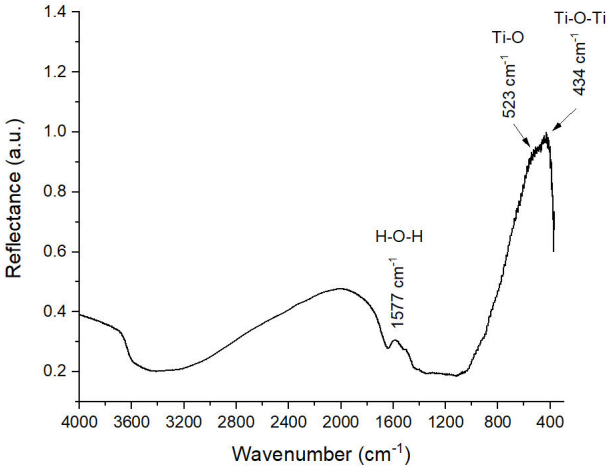

FIGURE 4. FT-IR spectrum of TiO_2. The Ti-O-Ti stretching vibration suggests the formation of TiO2.

measurements were performed to confirm the presence of amorphous TiO_2. Figure 4 shows the FT-IR spectrum of a TiO_2 layer. It can be observed that the vibrational mode at 900 cm^{-1}, corresponding to the first order stretching of the peroxo group (O-O) [28], is absent. Therefore, the thermal annealing at 120° after spin-coating deposition is sufficient to decompose and evaporate the peroxo group, resulting in TiO_2 that exhibits only the Ti-O-Ti stretching mode at 434 cm^{-1}, Ti-O stretching mode at 523 cm^{-1}. In addition, the band observed at 1577 cm^{-1} is attributed to H-O-H bending related to physisorbed water [36,37], which is commonly observed in amorphous TiO_2 due to surface hydroxylation and hydrogen bonding, with no evidence of other impurities that could reduce the transmittance of TiO_2 layers in the visible region evaluated in this research.

3.2. Optical characterization

Figure 5 displays the transmittance spectra of glass and a representative TiO_2 layer deposited on a glass substrate to ana-

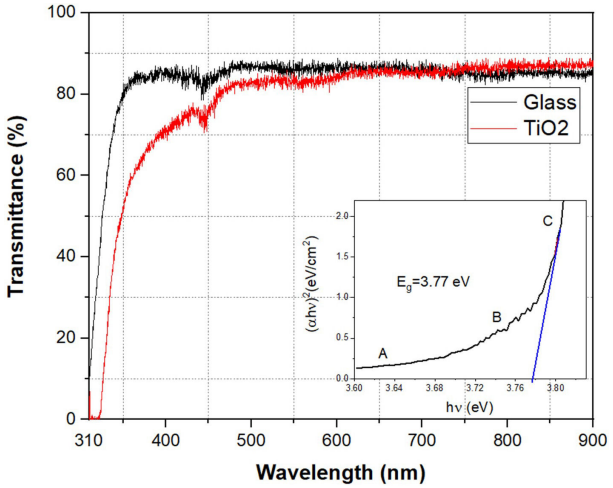

FIGURE 5. Comparison of the transmittance spectra of bare glass and TiO_2 deposited on glass. The inset illustrates the band gap calculation of TiO_2 using Tauc's method, along with the three characteristic absorption regions.

lyze its optical properties. It can be observed that the glass does not transmit light below 310 nm but from 365 nm the transmittance remains above 80%, while the transmittance spectrum of the TiO_2 sample deposited on glass does not transmit below 320 nm, but from 465 nm the transmittance increases above 80% absorbing only 20% of the radiation. This low absorbance is due to the bonds $\pi - \pi^*$ of the TiO_2, which cause energy absorption, because of the hybridization of 2p orbitals of oxygen and 3d orbitals of titanium that generate these bonds [38]. The high transmittance exhibited by the TiO_2 layer makes it suitable for application in OSCs, as UV light (320-400 nm), the entire visible spectrum, and IR light ($\geq$ 750 nm), are allowed to reach the absorber layer to generate electron-hole pairs. The inset in Fig. 5 describes the graph obtained using the Tauc method [39] to calculate the bandgap energy E_g of the TiO_2 layers. The bandgap energy was determined using the following equation

$$(\alpha h\nu)^n = B(h\nu - E_g), \tag{4}$$

where $h\nu$ is the photon energy, α is the absorption coefficient, B is a constant related to the electronic properties of the material and n is a value that depends on the nature of the material transition [39]. Because the amorphous TiO_2 is obtained by the sol-gel technique, we can see that the inset in Fig. 5 presents the characteristic curve for amorphous semiconductor materials with three regions: weak absorption zone (A), exponential zone (B), and high absorption zone (C) [40]. In the last zone, Tauc's method allows the determination of the E_g value by drawing a line from the zone C to the horizontal axis (inset of Fig. 5). The bandgap energy of the TiO_2 films was 3.77 eV, consistent with the amorphous nature of TiO_2 as confirmed by XRD and Raman spectroscopy results. The large band gap value of amorphous TiO_2 is due to the low annealing temperature (120°C) which allows neither the formation of large grains [40] nor the crystallization of TiO_2.

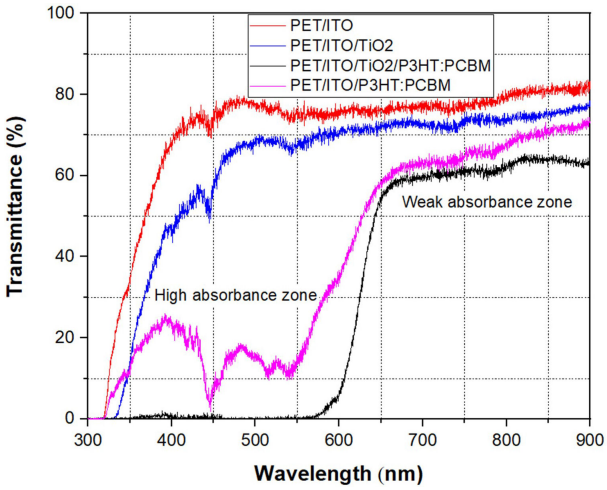

FIGURE 6. The transmittance spectrum of PET/ITO/TiO_2/P3HT:PCBM displays two absorption zones to improve the optical properties of OSC.

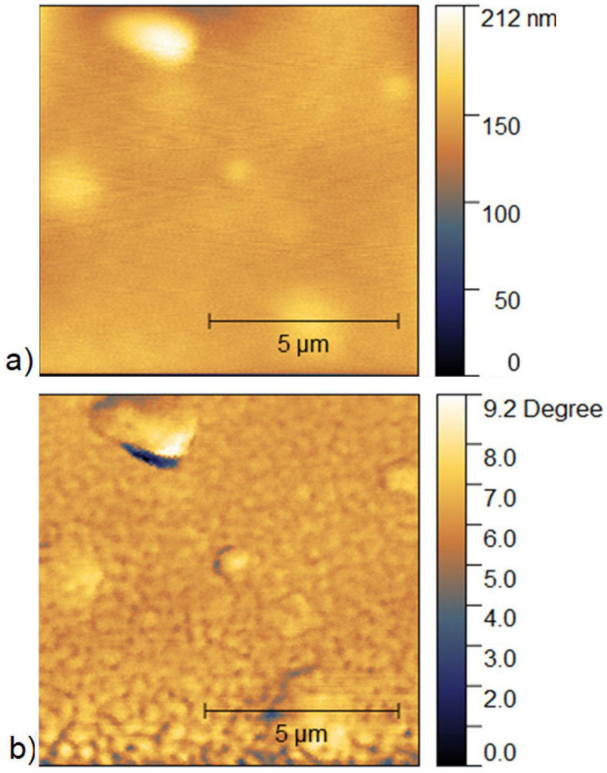

FIGURE 7. AFM images of P3HT:PCBM spin-coated onto TiO_2. a) Topography image showing a uniform distribution of P3HT:PCBM blend on TiO_2, b) Phase image showing typical morphology of the P3HT:PCBM blend on TiO_2.

It has been reported that the formation of TiO_2 crystals begins at 225°C, and it is fully crystallized into the anatase phase at 300°C [41].

Figure 6 shows the transmittance spectra of P3HT:PCBM deposited onto PET/ITO (labeled as PET/ITO/P3HT:PCBM), P3HT:PCBM deposited onto PET/ITO/TiO_2 (noted as PET/ITO/TiO_2/P3HT:PCBM), in comparison with a TiO_2 film deposited onto PET/ITO substrate (PET/ITO/TiO_2) and, bare PET/ITO. PET/ITO spectrum shows approximately 75% transmittance, in the 450-900 nm range, while the PET/ITO/TiO_2 spectrum exhibits a decrease in light transmittance. It can be observed that when the P3HT:PCBM is spin-coated onto the PET/ITO/TiO_2 structure, the transmittance drops to 0% in the 300-570 nm range (in contrast to PET/ITO/P3HT:PCBM), as an effect of the presence of the TiO_2 interlayer [42].

This result is significant, because it indicates a full absorption in the 400-570 nm wavelength range of visible electromagnetic radiation, which can lead to the generation of excitons and their dissociation into electrons and holes in the P3HT:PCBM based photovoltaic solar cells. Figure 6 also demonstrates that in the 660-900 nm range, a transmittance of 60% (40% absorbance) is maintained, being a zone that can also lead to the generation of excitons. According to other researchers [29], the observed absorbance is higher than the results in this research. Some reflection losses in the interfaces of the different layers may occur [43,44], but we consider them negligible compared to those in silicon solar cells [43].

AFM images of the P3HT:PCBM blend spin-coated on a TiO_2 layer are presented in Fig. 7. Figure 7a) shows that TiO_2 promotes the growth of smooth P3HT:PCBM layers without any cracks or holes. Figure 7b) displays the phase distribution of the two components of P3HT:PCBM, showing a uniform accommodation [45], thus demonstrating the effectiveness of the developed methodology for the fabrication of TiO_2 films through the spin-coating technique.

4. Conclusions

Amorphous TiO_2 was obtained by the sol-gel method and successfully deposited by the spin-coating technique at room temperature onto a flexible PET/ITO substrate to form the PET/ITO/TiO_2 structure. Raman spectroscopy results confirmed that TiO_2 was amorphous with an average particle size of 0.086 μm according to SEM analysis. The FT-IR spectrum of the TiO_2 layers exhibited only characteristic TiO_2 vibrational modes Ti-O (523 cm^{-1}) and Ti-O-Ti (434 cm^{-1}), confirming the chemical quality of the process. The energy value of the TiO_2 band gap was 3.77 eV, corresponding to amorphous TiO_2. The PET/ITO/TiO_2 system exhibited a transmittance of approximately 70% at 500 nm, making it a promising material for application in organic solar cells (OSCs).

P3HT:PCBM deposited on PET/ITO/TiO_2 exhibited almost 100% absorbance at 300-570 nm, but at 660-900 nm it showed a weak absorbance zone of about 40%. AFM images revealed a uniform distribution of TiO_2 deposited onto the PET/ITO, demonstrating a successful deposition of TiO_2 onto the PET/ITO substrate. Moreover, the typical P3HT:PCBM blend morphology was visible throughout the sample, demonstrating the formation of well-structured P3HT:PCBM layers capable of generating excitons in the absorber layer, thus contributing to the functionality of a flexible organic solar cell.

Acknowledgements

This work was partially supported by CONAHCYT under the PDCPN 2015 program (grant 28). C. Montero-Tavera acknowledges CONAHCYT-México for the postdoctoral scholarship *Investigadores por México 2022* (3) (CVU: 295183), conducted at the Department of Mechanical Engineering, Universidad de Guanajuato. The authors thank CINVESTAV-IPN Unidad Querétaro, LICAMM UG "Laboratorio de Investigación y Caracterización de Minerales y Materiales", and Instituto Politécnico Nacional campuses Altamira Tamaulipas and Ciudad de México for their support in material characterization.

Author contributions

C. Montero-Tavera: Investigation, methodology, validation, writing-original draft. M. Loeza-Poot: Methodology. M. Oviedo-Mendoza: Methodology, supervision. J. Moreno-Palmerín: Experimental resources. W. B. Rojas-Salinas: Laboratory resources. F. Caballero-Briones: Resources, M. Zapata-Torres: Resources. E. N. Hernández-Rodríguez: Conceptualization, supervision, funding acquisition, writing-review and editing.

1. A. J. Haider, Z. N. Jameel, and I. H. M. Al-Hussaini, Review on titanium dioxide applications, *Energy Procedia* **157** (2019) 17, https://doi.org/10.1016/j.egypro.2018.11.159
2. D. A. H. Hanaor and C. C. Sorrell, Review of the anatase to rutile phase transformation, *J Mater Sci* **46** (2011) 855, https://doi.org/10.1007/s10853-010-5113-0
3. P. Periyat, B. Naufal, and S. G. Ullattil, A review on high temperature stable anatase TiO2 photocatalysts, *In M S F*, **855** (2016) pp. 78-93, https://doi.org/10.4028/www.scientific.net/MSF.855.78
4. H. Zhang and J. F. Banfield, Thermodynamic analysis of phase stability of nanocrystalline titania, *J Mater Chem* **8** (1998) 2073, https://doi.org/10.1039/a802619j
5. B. Prasai, et al., Properties of amorphous and crystalline titanium dioxide from first principles, *J Mater Sci* **47** (2012) 7515, https://doi.org/10.1007/s10853-012-6439-6
6. L. M. Abadie and N. G. Larracoechea, Review and analysis of energy storage systems by hydro-pumping to support a mix of electricity generation with a high percentage of renewables, *Dyna* **94** (2019) 669, https://doi.org/10.6036/9182
7. E. Kabir, et al., Solar Energy: Potential and Future Prospects, *Renewable and Sustainable Energy Reviews* **82** (2018) 894, https://doi.org/10.1016/j.rser.2017.09.094
8. A. Kumar, M. Z. U. Khan, and B. Pandey, Wind Energy: A Review Paper, *GJET* **4** (2018) 29, https://doi.org/10.21058/gjet.2018.42004
9. P. A. Owusu and S. Asumadu-Sarkodie, A review of renewable energy sources, sustainability issues and climate change mitigation, *Cogent Engineering* **3** (2016) 1167990, https://doi.org/10.1080/23311916.2016.1167990
10. L. C. Andreani *et al*., Silicon solar cells: Toward the efficiency limits, *Advances in Physics: X* **4** (2019) 1548305, https://doi.org/10.1080/23746149.2018.1548305
11. M. B. de la Mora *et al*., Materials for downconversion in solar cells: Perspectives and challenges, *Sol Energy Mater Sol Cells* **165** (2017) 59, https://doi.org/10.1016/j.solmat.2017.02.016
12. O. A. Abdulrazzaq *et al.*, Organic Solar Cells: A Review of Materials, Limitations, and Possibilities for Improvement, *Particulate Science and Technology: An International Journal* **31** (2013) 427, https://doi.org/10.1080/02726351.2013.769470
13. X. Xu *et al*., Recent advances in stability of organic solar cells, *Energy-Chem* **3** (2021), https://doi.org/10.1016/j.enchem.2020.100046
14. L. Duan and A. Uddin, Progress in Stability of Organic Solar Cells, *Adv Sci* **7** (2020), https://doi.org/10.1002/advs.201903259
15. J. Kalowekamo and E. Baker, Estimating the manufacturing cost of purely organic solar cells, *Sol Energy* **83** (2009) 1224, https://doi.org/10.1016/j.solener.2009.02.003
16. M. Girtan, On the stability of electrical and photoelectrical properties of P3HT and P3HT:PCBM blends thin films, *Org Electron* **14** (2013) 200, https://doi.org/10.1016/j.orgel.2012.10 023
17. L. Hrostea *et al*., Optical and Morphological Properties of P3HT and P3HT:PCBM Thin Films Used in Photovoltaic Applications, *In IOP Conf Ser: Mater Sci Eng*, **374** (2018) p. 012015, https://doi.org/10.1088/1757-899X/374/1/012015
18. P. Vanlaeke *et al*., P3HT/PCBM bulk heterojunction solar cells: Relation between morphology and electro-optical characteristics, *Sol Energy Mater Sol Cells* **90** (2006) 2150, https://doi.org/10.1016/j.solmat.2006.02.010
19. S. L. Mousavi *et al*., Enhanced solar cell performance of P3HT:PCBM by SnS nanoparticles, *Sol Energy* **199** (2020) 872, https://doi.org/10.1016/j.solener.2020.02.031
20. H. Gao *et al*., Enhanced performance of polymer solar cells based on P3HT:PCBM via incorporating Au nanoparticles prepared by the micellar method, *J Mater Sci: Mater Electron* **31** (2020) 10760, https://doi.org/10.1007/s10854-020-03626-x
21. M. K. Omrani *et al*., Impact of hybrid plasmonic nanoparticles on the charge carrier mobility of P3HT:PCBM polymer solar cells, *Sci Rep* **11** (2021) 19774, https://doi.org/10.1038/s41598-021-99095-1

22. S. Bi *et al*., Physical properties of 2D and 3D ZnO materials fabricated by multi-methods and their photoelectric effect on organic solar cells, *J Sci: Advan Mater Dev* **3** (2018) 428, https://doi.org/10.1016/j.jsamd.2018.11.003

23. C. Chen and F. Li, Improving the efficiency of ITO/nc-TiO2/CdS/P3HT:PCBM/PEDOT:PSS/Ag inverted solar cells by sensitizing TiO2 nanocrystalline film with chemical bathdeposited CdS quantum dots, *Nanoscale Res Lett* **8** (2013) 453, https://doi.org/10.1186/1556-276X-8-453

24. E. Hernández-Rodríguez *et al*., Application of sputtered TiO2 thin films as HRT buffer layer for high efficiency CdS/CdTe solar cell, *Sol Energy* **132** (2016) 64, https://doi.org/10.1016/j.solener.2016.02.047

25. M. Boehme and C. Charton, Properties of ITO on PET film in dependence on the coating conditions and thermal processing, *Surf Coat Technol* **200** (2005) 932, https://doi.org/10.1016/j.surfcoat.2005.02.040

26. M. O. Abou-Helal and W. T. Seeber, Preparation of TiO2 thin films by spray pyrolysis to be used as a photocatalyst, *Appl Surf Sci* **195** (2002) 53, https://doi.org/10.1016/S0169-4332(02)00533-0

27. N. P. Poddar and S. K. Mukherjee, Characterization of TiO2 thin films deposited by using DC magnetron sputtering, *Carbon Sci Tech* **8** (2016) 1.

28. N. Sasirekha, B. Rajesh, and Y. W. Chen, Synthesis of TiO2 sol in a neutral solution using TiCl4 as a precursor and H2O2 as an oxidizing agent, *Thin Solid Films* **518** (2009) 43, https://doi.org/10.1016/j.tsf.2009.06.015

29. M. Oviedo-Mendoza *et al.*, Improving P3HT:PCBM absorber layers by blending TiO2/CdS nanocomposites for application in photovoltaic solar cells, *J Mater Sci: Mater Electron* **32** (2021) 102, https://doi.org/10.1007/s10854-020-04705-9

30. H. Ichinose, M. Terasaki, and H. Katsuki, Synthesis of Peroxo-Modified Anatase Sol from Peroxo Titanic Acid Solution, *Journal of the Ceramic Society of Japan* **104** (1996) 715, https://doi.org/10.2109/jcersj.104.715

31. B. A. Nejand, S. Sanjabi, and V. Ahmadi, Nanostructured phothocatalytic TiO2 thin film fabricated by magnetron sputtering on glass, *In Int J Mod Phys Conf Ser,* **05** (2012) p. 661, https://doi.org/10.1142/s2010194512002607

32. F. H. A. Bouabellou, Structural, optical and electrical properties of TiO2 thin films synthesized by sol-gel technique, *IOSR Journal of Engineering* **3** (2013) 21, https://doi.org/10.9790/3021-031112128

33. P. Francisco-Santiago, J. A. García-Macedo, and G. Valverde-Aguilar, Photoconductivity studies on amorphous and crystalline TiO2 and TiO2:Eu3+ thin films synthesized by sol-gel, In Nanophotonic Materials IX, International Society for Optics and Photonics (SPIE, 2012) p. 84560N.

34. I. M. Clegg *et al.,* On-Line Analysis Using Raman Spectroscopy for Process Control during the Manufacture of Titanium Dioxide, Appl Spectrosc **55** (2001) 1138, https://doi.org/10.1366/0003702011953388

35. A. A. Serkov *et al*., Laser sintering of gravure printed indium tin oxide films on polyethylene terephthalate for flexible electronics, *Sci Rep* **9** (2019), https://doi.org/10.1038/S41598-018-38043-Y

36. E. A. Al-Oubidy and F. J. Kadhim, Photocatalytic activity of anatase titanium dioxide nanostructures prepared by reactive magnetron sputtering technique, *Opt Quantum Electron* **51** (2019), https://doi.org/10.1007/s11082-018-1738-z

37. A. L. Hennemann *et al*., Amorphous Titanium Dioxide Nanoparticles and Their Unexpected Fragmentation in MALDI-TOF/MS, *ACS Omega* **9** (2024) 47831, https://doi.org/10.1021/acsomega.4c08770

38. H. Peng *et al*., First-principles study of the electronic structures and magnetic properties of 3d transition metal-doped anatase TiO2, *J Phys: Condens Matter* **20** (2008) 125207, https://doi.org/10.1088/0953-8984/20/12/125207

39. P. Makuła, M. Pacia, and W. Macyk, How To Correctly Determine the Band Gap Energy of Modified Semiconductor Photocatalysts Based on UV-Vis Spectra, *J Phys Chem Lett* **9** (2018) 6814, https://doi.org/10.1021/acs.jpclett.8b02892

40. M. L. Grilli *et al*., Room temperature deposition of XRDamorphous TiO2 thin films: Investigation of device performance as a function of temperature, *Ceram Int* **44** (2018) 11582, https://doi.org/10.1016/j.ceramint.2018.03.222

41. A. Jolivet *et al*., Structural, Optical, and Electrical Properties of TiO2 Thin Films Deposited by ALD: Impact of the Substrate, the Deposited Thickness and the Deposition Temperature, *Applied Surface Science* **608** (2023) 155214, https://doi.org/10.1016/j.apsusc.2022.155214

42. S. GÃ$\frac{1}{4}$nes, H. Neugebauer, and N. S. Sariciftci, Conjugated Polymer-Based Organic Solar Cells, *Chem Rev* **107** (2007) 1324, https://doi.org/10.1021/cr050149z

43. L. A. Kosyachenko, E. V. Grushko, and X. Mathew, Quantitative assessment of optical losses in thin-film CdS/CdTe solar cells, *Solar Energy Materials and Solar Cells* **96** (2012) 231, https://doi.org/10.1016/j.solmat.2011.09.063

44. E. Hernández-Rodríguez *et al*., A comparative study of CdS:F and CdS:O thin films deposited by reactive RF-sputtering technique for window layer application in solar cells, *Journal of Physics D: Applied Physics* **48** (2015) 255102, https://doi.org/10.1088/0022-3727/48/25/255102

45. J. M. Yun, D. Y. Kim, and Y. Y. Noh, Synthesis of fullerene derivatives for the application to organic photovoltaic cell and n-channel organic thin-film transistors, *Science of Advanced Materials* **8** (2016) 450, https://doi.org/10.1166/sam.2016.2537